Biomedical Optics EXPRESS

Standoff detection of biological agents using laser induced fluorescence—a comparison of 294 nm and 355 nm excitation wavelengths

Øystein Farsund,* Gunnar Rustad, and Gunnar Skogan

FFI (Norwegian Defence Research Establishment), Instituttveien 20, Kjeller, NO-2007, Norway
**oystein.farsund@ffi.no*

Abstract: Standoff detection measuring the fluorescence spectra of seven different biological agents excited by 294 nm as well as 355 nm wavelength laser pulses has been undertaken. The biological warfare agent simulants were released in a semi-closed aerosol chamber at 210 m standoff distance and excited by light at either of the two wavelengths using the same instrument. Significant differences in several of the agents' fluorescence response were seen at the two wavelengths. The anthrax simulants' fluorescence responses were almost an order of magnitude stronger at the shorter wavelength excitation. However, most importantly, the fluorescence spectra were significantly more dissimilar at 294 nm than at 355 nm excitation with ~7 nm spectral resolution. This indicates that classification of the substances should be possible with a lower error rate for standoff detection using 294 nm rather than 355 nm excitation wavelength, or even better, utilizing both.

OCIS codes: (170.6280) Spectroscopy, fluorescence and luminescence; (280.1100) Aerosol detection; (280.1415) Biological sensing and sensors; (280.3640) Lidar; (300.2530) Fluorescence, laser-induced.

References and links

1. S. D. Mayor, P. Benda, C. E. Murata, and R. J. Danzig, "Lidars: a key component of urban biodefense," Biosecur. Bioterror. **6**(1), 45–56 (2008).
2. J. Ho, "Future of biological aerosol detection," Anal. Chim. Acta **457**(1), 125–148 (2002).
3. "Laser Based Stand-Off Detection of Biological Agents. Final Report of Task Group SET-098/RTG-55," RTO-TR-SET-098 AC/323(SET-098)TP/265 (2010). *http://www.cso.nato.int/Pubs/rdp.asp?RDP=RTO-TR-SET-098*
4. R. Nyhavn, H. J. F. Moen, Ø. Farsund, and G. Rustad, "Optimal classification of standoff bioaerosol measurements using evolutionary algorithms," Proc. SPIE **8018**, 801806, 801806-13 (2011).
5. K. Baxter, M. Castle, S. Barrington, P. Withers, V. Foot, A. Pickering, and N. Felton, "UK small scale UVLIF lidar for standoff BW detection," Proc. SPIE **6739**, 67390Z, 67390Z-10 (2007).
6. T. Vo-Dinh, *Biomedical Photonics Handbook* (CRC Press, Boca Raton, FL, 2003).
7. J. R. Lakowicz, *Principles of Fluorescence Spectroscopy* (Kluwer Academic/Plenum, New York, 1999).
8. G. W. Faris, R. A. Copeland, K. Mortelmans, and B. V. Bronk, "Spectrally resolved absolute fluorescence cross sections for bacillus spores," Appl. Opt. **36**(4), 958–967 (1997).
9. Y. L. Pan, J. D. Eversole, P. H. Kaye, V. Foot, R. G. Pinnick, S. C. Hill, M. W. Mayo, J. R. Bottiger, A. L. Huston, V. Sivaprakasam, and R. K. Chang, "Bio-aerosol fluorescence," in *Optics of Biological Particles*, NATO science series, Vol. 238 of Series II, Mathematics, Physics and Chemistry, A. Hoekstra, V. Maltsev, and G. Videen, eds. (Springer, Dordrecht, 2007), pp 63–164.
10. P. Jonsson, F. Kullander, C. Vahlberg, P. Jelger, M. Tiihonen, P. Wasterby, T. Tjarnhage, and M. Lindgren, "Spectral detection of ultraviolet laser induced fluorescence from individual bioaerosol particles," Proc. SPIE **6398**, 63980F, 63980F-12 (2006).
11. Ø. Farsund, G. Rustad, I. Kåsen, and T. V. Haavardsholm, "Required Spectral Resolution for Bioaerosol Detection Algorithms Using Standoff Laser-Induced Fluorescence Measurements," IEEE Sens. J. **10**(3), 655–661 (2010).
12. P. Jonsson, M. Elmqvist, O. Gustafsson, F. Kullander, R. Persson, G. Olofsson, T. Tjarnhage, O. Farsund, T. V. Haavardsholm, and G. Rustad, "Evaluation of biological aerosol stand-off detection at a field trial," Proc. SPIE **7484**, 748400I (2009).
13. O. Farsund and G. Rustad, "Sum-Frequency Generation of High-Energy and High-Beam-Quality Ultraviolet Pulses," Int. J. Opt. **2011**, 737684 (2011).
14. G. G. Guilbault, *Practical Fluorescence* (M. Dekker, New York, 1990).

#175155 - $15.00 USD Received 30 Aug 2012; revised 15 Oct 2012; accepted 16 Oct 2012; pub. 24 Oct 2012

15. R. M. Measures, *Laser Remote Sensing—Fundamentals and Applications* (Krieger, Malabar, FL, 1992).
16. J. R. Simard, G. Roy, P. Mathieu, V. Larochelle, J. McFee, and J. Ho, "Standoff sensing of bioaerosols using intensified range-gated spectral analysis of laser-induced fluorescence," IEEE Trans. Geosci. Rem. Sens. **42**(4), 865–874 (2004).
17. S. C. Hill, R. G. Pinnick, S. Niles, Y.-L. Pan, S. Holler, R. K. Chang, J. Bottiger, B. T. Chen, C.-S. Orr, and G. Feather, "Real-time measurement of fluorescence spectra from single airborne biological particles," Field Anal. Chem. Technol. **3**(4-5), 221–239 (1999).
18. C. Laflamme, J. R. Simard, S. Buteau, P. Lahaie, D. Nadeau, B. Déry, O. Houle, P. Mathieu, G. Roy, J. Ho, and C. Duchaine, "Effect of growth media and washing on the spectral signatures of aerosolized biological simulants," Appl. Opt. **50**(6), 788–796 (2011).
19. M. Jerrett, R. T. Burnett, C. A. Pope 3rd, K. Ito, G. Thurston, D. Krewski, Y. L. Shi, E. Calle, and M. Thun, "Long-term ozone exposure and mortality," N. Engl. J. Med. **360**(11), 1085–1095 (2009).
20. D. B. Wetlaufer, *Ultraviolet Spectra of Proteins and Amino Acids*, Vol. 17 of Advances in Protein Chemistry (Academic, 1962), pp. 303–390.
21. MODTRAN, Air Force Research Labs, Hanscom AFB, MA, 2008.
22. Ø. Farsund, G. Arisholm, and G. Rustad, "Improved beam quality from a high energy optical parametric oscillator using crystals with orthogonal critical planes," Opt. Express **18**(9), 9229–9235 (2010).
23. S. Buteau, J.-R. Simard, and S. Rowsell, "Bioaerosols standoff detection simultaneously refereed with particle concentration (ppl) and viability units (ACPLA)," Proc. SPIE **7484**, 748408, 748408-12 (2009).
24. A. Furiga, G. Pierre, M. Glories, P. Aimar, C. Roques, C. Causserand, and M. Berge, "Effects of ionic strength on bacteriophage MS2 behavior and their implications for the assessment of virus retention by ultrafiltration membranes," Appl. Environ. Microbiol. **77**(1), 229–236 (2011).
25. International Standardisation Organisation, "Water Quality—Detection and Enumeration of Bacteriophages—Part 1: Enumeration of F-Specific RNA Bacteriophages," EN ISO 10705–1 (International Standardisation Organisation, Geneva, Switzerland, 1995).
26. V. Sivaprakasam, H. B. Lin, A. L. Huston, and J. D. Eversole, "Spectral characterization of biological aerosol particles using two-wavelength excited laser-induced fluorescence and elastic scattering measurements," Opt. Express **19**(7), 6191–6208 (2011).
27. V. Sivaprakasam, A. Huston, C. Scotto, and J. Eversole, "Multiple UV wavelength excitation and fluorescence of bioaerosols," Opt. Express **12**(19), 4457–4466 (2004).
28. C. Laflamme, J.-R. Simard, S. Buteau, P. Lahaie, D. Nadeau, B. Déry, O. Houle, P. Mathieu, G. Roy, J. Ho, and C. Duchaine, "Effect of growth media and washing on the spectral signatures of aerosolized biological simulants," Appl. Opt. **50**(6), 788–796 (2011).
29. Y. L. Pan, S. C. Hill, R. G. Pinnick, H. Huang, J. R. Bottiger, and R. K. Chang, "Fluorescence spectra of atmospheric aerosol particles measured using one or two excitation wavelengths: comparison of classification schemes employing different emission and scattering results," Opt. Express **18**(12), 12436–12457 (2010).
30. H. C. Huang, Y. L. Pan, S. C. Hill, R. G. Pinnick, and R. K. Chang, "Real-time measurement of dual-wavelength laser-induced fluorescence spectra of individual aerosol particles," Opt. Express **16**(21), 16523–16528 (2008).
31. M. Seaver, D. C. Roselle, J. F. Pinto, and J. D. Eversole, "Absolute emission spectra from Bacillus subtilis and Escherichia coli vegetative cells in solution," Appl. Opt. **37**(22), 5344–5347 (1998).
32. T. V. Haavardsholm, Ø. Farsund, and G. Rustad, "Biological aerosol standoff detection and agent discrimination based on experimental UV laser induced fluorescence data," presented at *2008 Algorithm Workshop*, DTRA and JSTO (Baltimore, MD, Nov. 4–6, 2008).

1. Introduction

Standoff detection of biological aerosols (bioaerosols) has been identified as an important means to reduce the consequences of an eventual bioaerosol attack, due to its early warning capability [1], and it also has significant potential in environmental monitoring [2]. The majority of current standoff instruments detect aerosolized biological agents using ultraviolet laser induced fluorescence (UVLIF) [3]. While early instruments measured the fluorescence in one or a few spectral bands, modern instruments tend to have greater spectral resolution [4,5]. These instruments commonly use the third or fourth harmonic of a Q-switched Nd:YAG laser as excitation source. Such a laser and harmonic stages are commercially available and deliver pulses of appropriate duration and sufficient energy for detection up to about one km standoff distance. However, there are drawbacks with the commercially available wavelengths. While excitation wavelengths around 350 nm seem to be customary [3], the most important naturally occurring fluorophores, tryptophan, phenylalanine and tyrosine, absorb most efficiently at wavelengths considerably shorter than 355 nm [6, p. 3-17], [7, p. 65]. At the fourth harmonic of Nd:YAG (266 nm), on the other hand, absorption by atmospheric ozone close to the ground can dramatically reduce standoff distance. More specifically, based on laboratory measurements at several excitation wavelengths, the region

#175155 - $15.00 USD Received 30 Aug 2012; revised 15 Oct 2012; accepted 16 Oct 2012; pub. 24 Oct 2012

around 280 nm has been held to be more efficient in terms of excitation for fluorescence than 355 nm [6, p. 28-12], [8–10].

FFI has previously developed a UVLIF standoff instrument using a 355 nm laser light source for the excitation of the bioaerosols with high spectral resolution of the detected fluorescence. This biological lidar instrument (hereafter *biolidar*) was used in several field experiments [11,12]. Recently, a compact 294 nm pulsed laser source was developed by means of nonlinear conversion of a commercial Nd:YAG laser [13]. This source was integrated in the lidar instrument, and standoff detection experiments using a semi-closed release chamber were carried out. Seven different agents used for the simulation of biological warfare agents (BWA) were released at 210 m standoff distance, and their fluorescence spectra when excited at the two different wavelengths were measured at standoff distance.

In the following, we give a brief theoretically based motivation for choosing a more difficult accessible excitation wavelength, followed by a description of the lidar instrument and the experimental setup. Finally, the measurement results are presented, discussed and compared to single aerosol particle measurements reported by others.

2. Theory and motivation

The fact that some parts of the biological material emit fluorescence when exposed to ultraviolet light is utilized [6, p. 3-17], [7, p. 63], [14, pp. 575, 776]. The biolidar uses range-gated, ultraviolet laser induced fluorescence to detect biological aerosols at a distance. Assuming a laser emitting a pulse propagating through a column of air before being inelastically scattered by aerosols within a probe volume confined by the field of view (perfectly overlapping the laser beam) and range gating, the return signal impinging the ICCD camera, can be described by a simplified form of the lidar equation [15, pp. 237–256], [16]:

$$E(\lambda, r) = E_L K_0(\lambda) T(\lambda, r) \frac{A_0}{r^2} N(r) \frac{\sigma^F(\lambda_L, \lambda)}{4\pi} \frac{c\tau_d}{2} \qquad (1)$$

The intention of this work was to investigate the fluorescence response in terms of magnitude and spectral features as function of two different excitation (laser) wavelengths (λ_L). Experiments allow for good control over several parameters; the laser pulse energy (E_L), geometry (area of collecting optics, A_0, and standoff distance, r) and detector integration time (τ_d). The number density of aerosol particles in the probed volume (N) can be measured indirectly for example by a particle counter or slit sampler. Based on instrument component specifications, the instrument spectral response (K_0) may be calculated. We are thus able to measure a combination of the fluorescence scattering cross section (σ^F) with atmospheric transmission (T) and other inelastic scattering processes, such as Raman scattering, isolating it from instrument characteristics and normalized with respect to a measure of aerosol scatterers.

The main reason for using 355 nm laser light is that it is easily available through third harmonic generation of the 1064 nm pulses from a Nd:YAG laser. The main substance that fluoresces after 355 nm excitation is the molecule NADH. This is the reduced form of nicotinamide adenine dinucleotide (NAD^+), and is important in cell respiration and hence metabolism. NADH is therefore present in bacteria and other living cells [14, p. 776], but to a lesser degree in spores or viruses. We have previously seen that the fluorescence following 355 nm excitation of various substances exhibit sufficient dissimilarities that the different substances can be classified [4,11,12], but it is a challenging task as the differences between the fluorescence spectra are relatively small. It is well known that the growth medium and the preparation the agents will influence the spectral signatures; and thereby distort the ability to discriminate agents [17,18]. The effects of the growth medium and agent preparation have not been studied in the present work. Among the most important biological fluorophores, tryptophan is not excited in the 355 nm laser approach because tryptophan requires excitation at wavelengths below ~310 nm [6, p. 28–12], see Fig. 1 (a). As tryptophan is an amino acid and therefore present in all biological material, this is an important limitation of the 355 nm excitation scheme. Tryptophan can be excited with laser pulses at 266 nm, which is the fourth

#175155 - $15.00 USD Received 30 Aug 2012; revised 15 Oct 2012; accepted 16 Oct 2012; pub. 24 Oct 2012

harmonic of the Nd:YAG laser, and this has been used in some instruments [5]. However, presence of ozone close to the ground will absorb this wavelength. For example, at 100 ppb O_3 concentration, which can occur in urban areas in the summer [19], 266 nm light experiences ~90% loss per km. For comparison, at 280 nm and 290 nm, the corresponding loss is ~60% and ~30%, respectively, which affects the lidar return signal accordingly (through T(λ,r) in Eq. (1)), see Fig. 1 (b). As the absorption cross section for tryptophan is significantly larger for 280 nm than 266 nm, it is of interest to examine wavelengths in the 280-290 nm range for their suitability in standoff detection of biological aerosols. This has been the topic of this work.

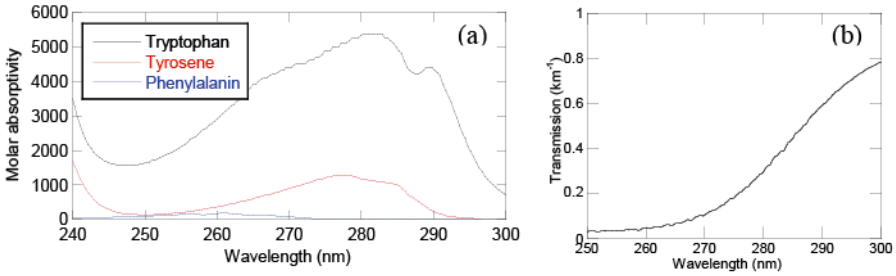

Fig. 1. (a) Absorption spectra for the most important fluorescing amino acids; tryptophan, tyrosine and phenylalanine (spectra taken from [20]). (b) Calculated transmission through 1 km of USTD atmosphere with 100 ppb O_3 using MODTRAN [21].

3. Experiment

3.1 Lidar

A sketch of the FFI biolidar and its key figures used during the experiment are shown in Fig. 2. Laser light is sent out on-axis of the optical telescope that collects the return fluorescence. This is spectrally resolved through a spectrograph and detected with a range gated intensified CCD (ICCD) camera with ~7 nm spectral resolution [12].

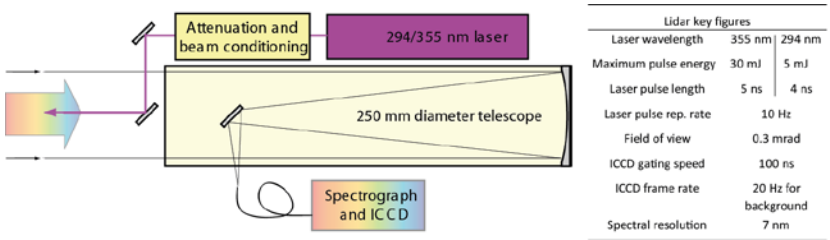

Lidar key figures		
Laser wavelength	355 nm	294 nm
Maximum pulse energy	30 mJ	5 mJ
Laser pulse length	5 ns	4 ns
Laser pulse rep. rate	10 Hz	
Field of view	0.3 mrad	
ICCD gating speed	100 ns	
ICCD frame rate	20 Hz for background	
Spectral resolution	7 nm	

Fig. 2. Sketch of the lidar and its key figures. Pulse energy levels were restricted because of unstable Nd:YAG laser operation at high pulse energies during field use.

Both the fundamental wavelength and the frequency tripled output from a frequency tripled flash-lamp pumped Nd:YAG laser was used to extend the capacity to shorter wavelength UV. We used an optical parametric oscillator (OPO) pumped by the laser fundamental wavelength to generate 1.7 µm radiation, with which 294 nm was generated by sum frequency mixing with 355 nm using a nonlinear crystal (BBO) [13]. The beam quality was suitable for stand-off detection owing to the orthogonal critical planes geometry used in the large-beam OPO [22]. Ideally, an even shorter UV wavelength is preferential, but transmission properties in the optical materials in the current setup limited the wavelength to 294 nm. Both the 294 nm beam and the 355 nm beams could be used as the lidar excitation source. Minor modifications to the setup would allow for automatic dual wavelength operation, for example shot-to-shot alteration. The optical layout is shown in Fig. 3(a).

The ICCD camera gating was set according to the distance to and size of the aerosol release chamber, to approximately 100 ns which was significantly greater than the pulse

#175155 - $15.00 USD Received 30 Aug 2012; revised 15 Oct 2012; accepted 16 Oct 2012; pub. 24 Oct 2012

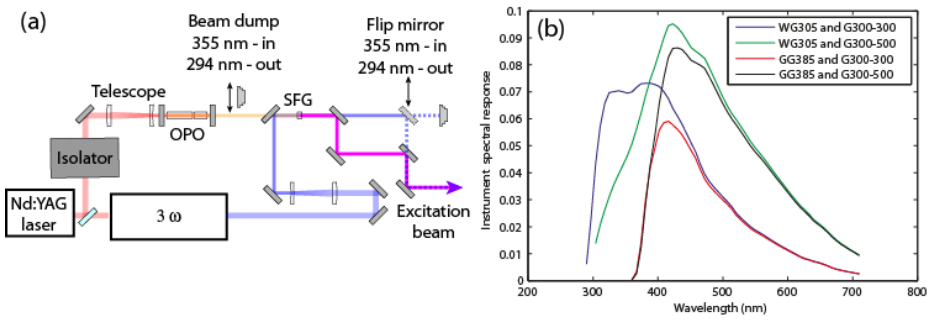

Fig. 3. (a) Excitation laser of the lidar. A 294 nm beam was generated by sum frequency mixing the 1.7 μm OPO signal with the third harmonic (355 nm) of the laser. 294 nm or 355 nm excitation wavelength was selected by adjusting the flip mirror and beam dump, as is explained in the figure. (b) Calculated instrument spectral responses of the biolidar for the four different combinations of color glass filter and grating used, including the ICCD quantum efficiency.

length and the biological aerosol fluorescence life time (approximately 3.1 ns and 0.4 ns for tryptophan and NADH, respectively [7, pp. 63–64, 488]). The average laser power was measured immediately prior to dissemination of the agent. During 294 nm operation, the output pulse energy was 3-5 mJ, whereas approximately 30 mJ was used during 355 nm operation. These levels were used to allow for stable operation. We have demonstrated more than 25 mJ operation of the 294 nm light source in a fine-tuned experiment in the laboratory [13]; however, unstable operation of the commercial frequency tripled Nd:YAG laser with changing ambient temperature affected the stability of the UV pulse energy severely. The Andor Shamrock 163i spectrograph was employed with either one of two different gratings during the experiment, both with 300 lines/mm ruling, but with different blaze angles (optimized for transmission at 300 nm and 500 nm, respectively). To reduce elastic backscatter levels to avoid saturation of the Andor DH720-18H-83 ICCD camera, WG 305 and CVI LP385 (corresponds to Schott GG385) color glass filters were used for 294 nm and 355 nm excitation, respectively. The calculated total instrument spectral responses for the four different configurations (including mirrors, optical fiber and camera) corresponding to K_0 of Eq. (1), are shown in Fig. 3(b). All spectra presented in Figs. 9–10 have been corrected for the corresponding spectral response. The camera operated at twice the 10 Hz laser pulse repetition rate to acquire one background spectrum for each fluorescence spectrum. The measured spectrum was corrected on the fly.

3.2 Agent dissemination and referencing

The 5 m long semi-closed release chamber had 1 m × 1 m air curtains at each end to confine the aerosols within the chamber without the use of windows (windows would have rendered the measurements impossible as they fluoresce significantly after UV excitation). The laser diameter was only about 100 mm inside the chamber, thus filling the entire chamber with aerosols would be needless in terms of amount of agent use and time to fill and evacuate the chamber. We therefore fixed a 500 mm diameter and 3 m long ventilation duct between the air curtains of the container, into which the agents were released using aerosol generators and a fan placed at the far end (with respect to the lidar), see Fig. 4(a). The particle concentration inside the duct was monitored by means of an Aerodynamic Particle Sizer (APS 3321 from TSI Inc), which had its inlet located half way down the duct; see Fig. 4(b).

The APS measured the aerodynamic diameter distribution of the aerosols. A background measurement was carried out prior to the release. The background was subtracted from the measurement carried out during the release, giving us a reference for the particle number and size distribution of the dissemination. The integral over all particle sizes released was used for reference (which measures the particle concentration, “particles per liter air,” *ppl*), as a slit

#175155 - $15.00 USD Received 30 Aug 2012; revised 15 Oct 2012; accepted 16 Oct 2012; pub. 24 Oct 2012

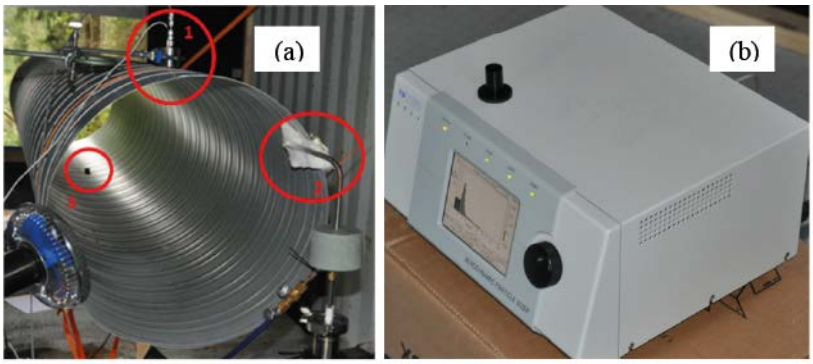

Fig. 4. (a) Ø500 mm duct through which the lidar was directed, and into which the aerosols were released either wet (1) or dry (2). (b) The APS measured the aerosol size distribution, and was located with its inlet protruding into the pipe (position 3 in Fig. 4(a)).

sampler (which gives measurements of viability units, "Agent Containing Particles per Liter of Air," *ACPLA*) was not used in the experiments. UVLIF standoff measurements refereed with particle concentration and viability units have been reported, and the *ACPLA* to *ppl* ratio in their experiments varied between 1% and 30% [23].

Agents dissolved in water solution were disseminated using a 48 kHz ultrasonic spray nozzle (from Sono-Tek Corporation). Dry agents were released using custom built gear. The lidar was located at 210 meters distance from the release chamber, see Fig. 5. The laser beam was centered in the test tube and both the 355 nm and 294 nm beams had diameters of approximately 10 cm inside the chamber.

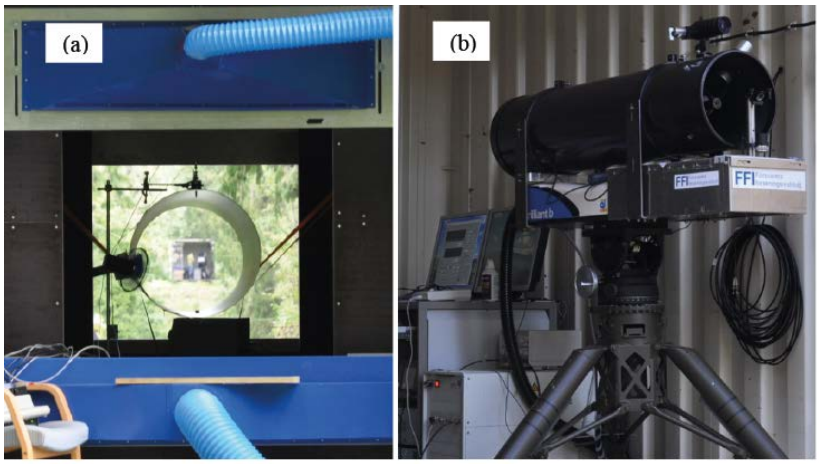

Fig. 5. (a) The lidar as seen through the release chamber, 210 m behind. The size of the laser beam inside the test chamber was about 100 mm diameter, i.e., significantly smaller than the 500 mm cross section of the release duct. (b) Photo of the FFI biolidar.

3.3 Biological agents disseminated in the experiments

Seven different agents were released during the experiments. BG is spores of *Bacillus atrophaeus*. The spores originate from *Dugway Proving Ground*, batch #026, lot #19076-03268. The spores were suspended in deionized water at a concentration of 8 mg/ml. BG spores are commonly used as a BW simulant for *Bacillus anthracis* spores. BT is spores of *Bacillus thuringiensis* (we used a commercial preparation called Turex, normally used as a biological insecticide). BT is another simulant for anthrax spores. EH is *Pantoea agglomerans*, originating from the *American Type Culture Collection* (ATCC 33243). The

#175155 - $15.00 USD Received 30 Aug 2012; revised 15 Oct 2012; accepted 16 Oct 2012; pub. 24 Oct 2012

culture was cultivated overnight at 30°C in nutrient broth from Merck (5.0 g/l peptone from meat and 3.0 g/l meat extract). EH was used as a simulant for pathogenic gram-negative bacteria, like *Francisella tularemia* (rabbit fever) and *Yersinia pestis* (plague). *E.coli* is the gram negative bacterium *Escherichia coli*, from *Deutsche Sammlung von Mikroorganismen und Zellkulturen* (DSM 4230). This culture was also grown at 30°C overnight in nutrient broth. *E.coli* can be used as a simulant for pathogenic gram-negative bacteria. MS2 is a bacteriophage, i.e., a virus infecting bacteria. MS2 was inoculated into a log phase *E.coli* culture (DSM 5695) and grown overnight at 37°C in LB medium (10 g/l tryptone, 5 g/l yeast extract and 10 g/l NaCl). After cultivation, bacteria were removed by centrifuging at 2000 *g* for ten minutes, followed by filtration using a 0.2 µm filter (from Whatman) [24]. The bacteriophage MS2 was enumerated according to the double-layer-agar method [25]. MS2 is used as a simulant for pathogenic viruses, e.g. smallpox or ebola. OA is ovalbumin. We used OA named Sigma-Aldrich A5253. Fumed silica, Sigma-Aldrich S5505, was added in a concentration of 1% to make the OA more "volatile". Ovalbumin is used as a simulant for toxins, e.g. ricin. SM is *Serratia marcescens* originating from *Collection de Institut Pasteur* (CIP 53.90). The culture was grown overnight at 30°C in nutrient broth. SM was used as a simulant for pathogenic gram-negative bacteria. All agents were released in an aqueous solution (deionized water), except for BT and OA, which were disseminated dry (powder).

4. Results

The aim of the experiments was to compare the fluorescence spectra in terms of responsivity and spectral features as function of the laser excitation wavelength and pulse energy. The return spectrum between 280 nm and 630 nm was measured with the camera. As this could potentially lead to problems with overlapping of the second order of the high frequency part of the spectrum with the first order of the low frequency part in the spectrograph, we chose to only regard the 280-560 nm spectral range when exciting the agent at 294 nm. For 355 nm excitation we used data up to 610 nm. Our previous measurements at 355 nm excitation have shown that the spectral range above ~600 nm does not contain useful information (see also measured results in [6, p. 28-12], [9]).The raw data consisted of 205 channels at 10 Hz sample rate. An example of the raw data acquired during the release of OA is shown in Fig. 6(a).

The time-averaged spectrum in Fig. 6(b) is from a time interval with weak fluorescence signal and shows several distinct lines. The spikes seen in the measured spectra do not originate from the fluorescence of the agent in consideration. First of all, elastic scattering at the laser wavelength is seen even though the radiation at the excitation wavelength is attenuated by several orders of magnitude. Moreover, Raman-scattering of atmospheric constituents, in particular for N_2 shifting the wavenumber by 2330 cm^{-1} [15, p. 107] (to approximately 315 nm for 294 nm excitation), are inevitable. 355 nm elastic scattering also appears when operating the lidar at 294 nm, because our source uses 355 nm to generate the

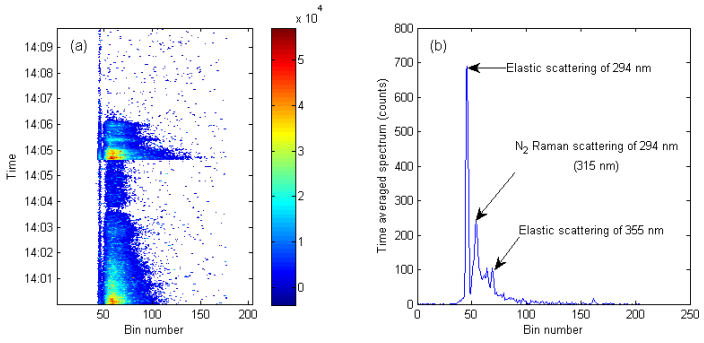

Fig. 6. (a) Example of raw data during measurement with 294 nm excitation and dissemination of OA (recorded fluorescence spectra as function of time). Color coding indicates signal strength (counts), and a bin corresponds to a spectral channel. (b) Time average of the spectra measured between 14:07 and 14:09 as shown in (a) (i.e., at weak measured fluorescence).

#175155 - $15.00 USD Received 30 Aug 2012; revised 15 Oct 2012; accepted 16 Oct 2012; pub. 24 Oct 2012

294 nm radiation. The optical leakage at 355 nm is less than 10^{-5}, but still sufficiently large that the elastic backscatter be comparable with the fluorescence following 294 nm excitation. The locations of these lines were used to calibrate the wavelength axis. The spectral features of the agents were extracted from measurements during intervals of considerable fluorescence signal and correspondingly high particle counts on the APS reference instrument, disregarding intervals with little or no fluorescence.

4.1 Response linearity with respect to agent quantity

An important assumption when averaging spectral features at different agent concentration levels, is that the features, or shape, of the fluorescence spectrum are the same for different quantities of aerosols in the measurement volume. This is tantamount to operating the laser power below a certain threshold, where fluorescence intensity is proportional to the illumination [9]. Sivaprakasam *et.al* showed that the fluorescent emission of bioaersols was linear with the incident laser fluence up to several mJ/cm^2 in experiments on individual bioaerosol particles [26]. The average of the currently measured spectra at significantly different agent concentration levels are plotted in Fig. 7(a) and normalized with respect to the particle concentration measured by the APS in Fig. 7(b).

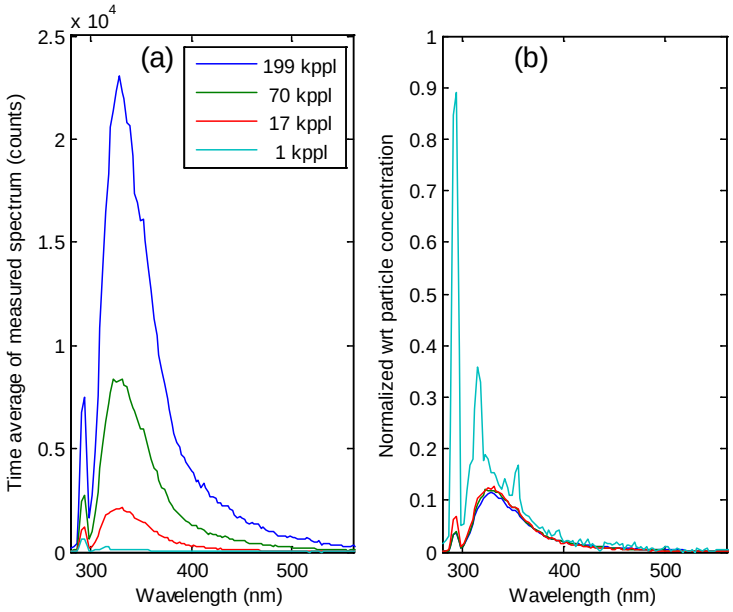

Fig. 7. (a) Spectral average of measurements acquired during different particle concentration levels (average of measured particle concentration during the acquisition); different agent concentration levels impose different signal levels. (b) Spectra normalized with respect to the particle concentration as measured by the APS coincide at different agent concentrations until the signal approaches background level, where other effects become prominent (same color coding as in (a)).

The similar spectral shapes indicate that the assumption is appropriate also in the current measurements. At low signal level we recognize the characteristic spikes related to elastic backscatter and Raman-scattering. The result is also important for the estimation of agent quantity within the probe volume, as determined by the laser cross section (or field of view if it is smaller) inside the gating depth.

4.2 Agent spectra at different excitation wavelengths

The most important parameter for the selection of excitation wavelength in terms of standoff detection sensitivity is the fluorescence cross section of the agent in consideration, σ^F of Eq.

#175155 - $15.00 USD Received 30 Aug 2012; revised 15 Oct 2012; accepted 16 Oct 2012; pub. 24 Oct 2012

(1), which depends on aerosol particle size. Sivaprakasam *et.al* measured laser induced fluorescence of single aerosol particles, and showed that the elastic and fluorescence scattering scale similarly with particle size, thus the size dependence may be eliminated by normalizing the fluorescence signal by the elastic scattering [26,27]. Our setup used several different combinations of color glass filters and diffractive gratings; hence was not optimized for measuring the elastic scattering. Moreover, in a standoff setting, the elastic scattering will be influenced by background aerosols in the measurement path. The APS for particle reference, measured the size distribution of all particles (not only the fluorescent ones) at a single point in the probe volume, and consequently did not provide adequate information on the distribution of disseminated aerosols in the probed volume to find N of Eq. (1). Figure 8 (a) shows an example of the measured total fluorescence when the aerosols were excited at 294 nm. Also shown is the particle concentration, meaning the integral of all aerodynamic diameters, as measured by the APS during a substantial release of OA. The APS and fluorescence curves correlate well taking into account that the APS has a much lower sampling rate than the standoff instrument, and the fact that the APS measured at one point location within the probed volume. The atmospheric effects in the fluorescence spectral interval may be neglected for relevant standoff distances. Transmission curves through various distances of standard atmosphere (7°C temperature, 85% relative humidity, 3 m above ground) were calculated using MODTRAN [21], see Fig. 8(b).

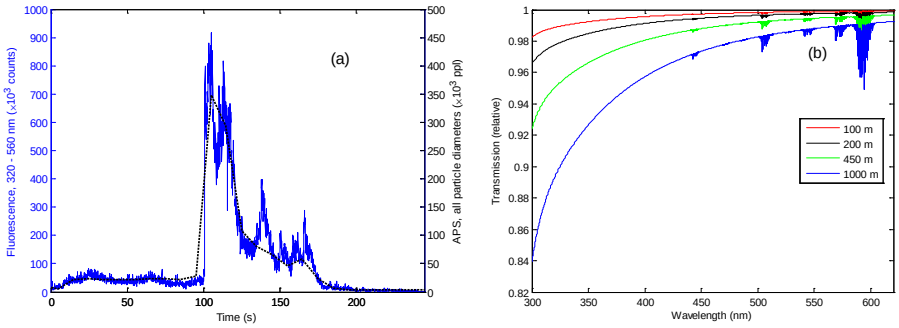

Fig. 8. (a) Comparison of measured fluorescence in the spectral range 320-560 nm (blue) and total number of particles (integrated over all aerodynamic diameters) as measured by the APS (dashed black), acquired during the release of OA while operating the lidar with the 294 nm excitation source. (b) Atmospheric influence on fluorescence spectral interval as calculated by MODTRAN, after propagation through 100 m, 200 m, which was the distance used in the experiment, 450 m and 1000 m atmosphere. See text for atmospheric parameters used in the simulations.

Therefore, in this section we present the spectra corrected for the instrument spectral response, and normalized with respect to laser pulse energy and the measured concentration of disseminated particles, as explained above, for the two excitation wavelengths, see Fig. 9. The anthrax simulants BG and BT fluoresce significantly stronger when excited by 294 nm than 355 nm. When exciting the aerosolized agents by a given pulse energy, the fluorescence is 6-8 times more intense at 294 nm than 355 nm laser wavelength. The strong 355 nm signal in the 294 nm excitation curve stems from backscattered 355 nm light that was not sufficiently attenuated before directing the pulse along the optical axis of the telescope. The fluorescence from an aerosol containing EH has approximately the same magnitude for both excitation wavelengths. Like for *E.coli*, it also seems clear that there is significant NADH content in the cells. MS2 is a simulant for BWA in the form of virus. The magnitudes of the spectra are similar for the two excitation wavelengths. The bacteriophage MS2 is a virus that infects *E.coli*. The solution was filtrated using a 0.2 µm filter before it was released in order to remove the *E.coli* bacteria. The fluorescence at 355 nm excitation indicates presence of NADH, related to metabolism which does not take place in virus. On the other side, the bacteria, and thus NADH, should have been significantly reduced by centrifuging and

#175155 - $15.00 USD Received 30 Aug 2012; revised 15 Oct 2012; accepted 16 Oct 2012; pub. 24 Oct 2012

filtration. However, the growth medium and NADH from damaged *E.coli* cells may be dissolved and pass filtration. OA is a simulant for toxins, and contains ~1% tryptophan [7, p. 445]. We therefore expected significantly stronger fluorescence at 294 nm than at 355 nm. Indeed it is stronger, however only by a factor of two. 294 nm excited SM fluoresces about twice as strongly as if excited at 355 nm.

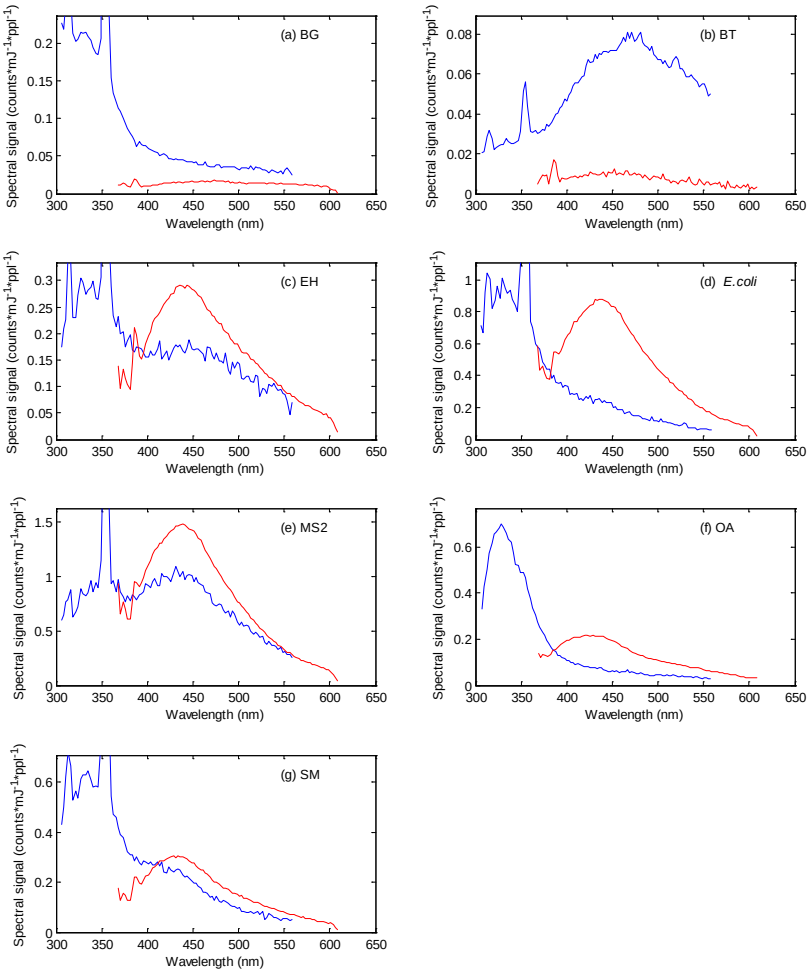

Fig. 9. Measured fluorescence following excitation by 294 nm (blue) and 355 nm (red) pulses for different aerosolized biological agents; (a) BG, (b) BT, (c) EH, (d) *E.coli*, (e) MS2, (f) OA and (g) SM. The spectra have been corrected for instrument spectral response, excluding ICCD gain, which was set to maximum, (approximately 800x), during all measurements. The fluorescence levels have been normalized with respect to laser pulse energy and particle concentration level.

4.3 Comparison of agent spectra at equal excitation wavelength

The magnitude of the fluorescence response as function of the excitation wavelength is an important parameter for the choice of laser wavelength. However, in terms of the ability to discriminate between different agents, the dissimilarities of the spectral features are crucial. In Fig. 10, the spectra for all the different agents at equal excitation wavelength are shown. The spectra were arbitrarily normalized for the purpose of comparing shapes.

As discussed at the beginning of this section, the spikes seen in the spectra are other effects than fluorescence from the agents. By visual comparison, an excitation wavelength at

#175155 - $15.00 USD Received 30 Aug 2012; revised 15 Oct 2012; accepted 16 Oct 2012; pub. 24 Oct 2012

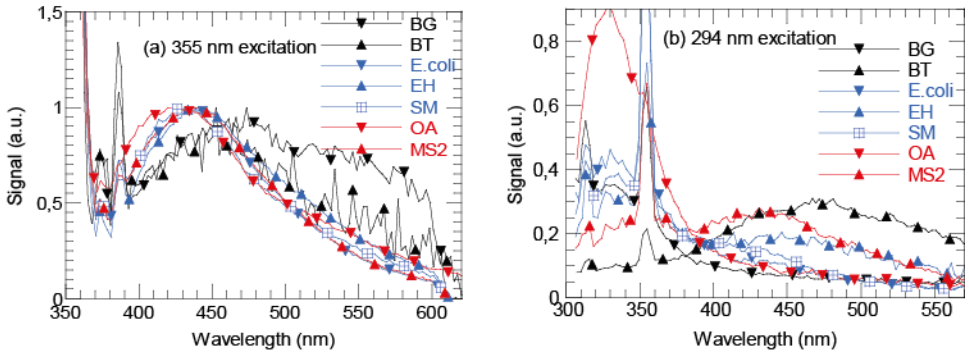

Fig. 10. Fluorescence spectra corrected for instrument spectral response, and normalized in order for visual comparison of shape for the seven different agents when excited by (a) 355 nm and (b) 294 nm radiation.

294 nm seems to generate more distinct fluorescence spectra than 355 nm excitation does. In the latter case, classification using benchmark methods, such as principal components analysis and support vector machines, is demanding due to the similarity of the spectra for the different agents. However, a genetic algorithm employed to the same data set outperformed classical methods in terms of false alarm rate [4]. The considerably larger variation in spectra with 294 nm excitation implies that we should expect even better classification results, meaning lower false alarm rates in terms of standoff detection performance at comparable laser pulse energies. However, classification has not been a topic of this work.

The fluorescence spectra are influenced by the growth media, and the preparation of the bioaerosol [9,17,26,28]. This has not been investigated in the experiments presented herein, but we note that EH, *E.coli*, SM (and MS2) which were cultivated using the same growth medium, and prepared in the same way, all have very similar fluorescence spectra after 355 nm excitation. The 294 nm excited spectra, on the other hand, possess more distinct spectral features. This observation favors the use of the shorter excitation wavelength.

4.4 Comparison of agent spectra with other publications

Fluorescence spectra of the same biological agents as studied in the current work have been presented in several publications. However, these are measurements of individual aerosol particles [29,30], or close-up laboratory measurements of aqueous solutions and aerosols [8,31], carried out at a number of different excitation wavelengths. When comparing these close-up spectra to standoff spectra, effects such as Raman scattering by atmospheric nitrogen, and in our case, 355 nm elastic scattering in the 294 nm excitation scheme, have to be taken into account. By doing this, the spectra compare well. This applies to the BG spectra (*Bacillus subtilis* compared with *Bacillus atrophaeus*), *E.coli* and albumin (albumin compares well to ovalbumin, whereas the bovine serum albumin spectrum is shifted to longer wavelengths), whereas the bacteriophage MS2 spectra [29] differ significantly for both excitation wavelengths. This may be attributed to fluorescence from the growth medium and aerosol preparation as discussed in Sec. 4.2.

4.5 Factors affecting signal-to-noise-ratio

In a system for standoff detection, several factors influence on the system performance. Our system corrects for background light on the fly by acquiring spectra at twice the laser pulse rate and subtracting the passive from the active spectrum. The noise level (or background level) of the system is strongly affected by ambient light and also of the gating time of the ICCD camera. With the settings used in this work, the rms background signal was about 30-150 counts/pulse per channel when operating under varying daylight conditions with a short gating time. A longer gating time, as would typically be used in open field surveillance, would

#175155 - $15.00 USD Received 30 Aug 2012; revised 15 Oct 2012; accepted 16 Oct 2012; pub. 24 Oct 2012

increase this accordingly. At low ambient light conditions, however, the background signal will be significantly smaller.

The signal, on the other hand, depends linearly with laser energy and with area of the collecting aperture, and is inversely proportional to the square of the standoff distance. The signal-to-noise (or signal-to-background) ratio can also be improved by reducing the spectral resolution. We have previously shown for a 355 nm based lidar that the number of spectral channels can be reduced to 10-15 before the signal processing performance with respect to false alarm or false negative is affected [4,11,32]. Such an analysis has not been a part of this work, but it seems likely that the more distinct fluorescence spectra with 294 nm excitation may see a similar or even smaller requirement for spectral channels.

5. Conclusion

The experiments verified that ultraviolet laser induced fluorescence featuring excitation by a laser with wavelength 294 nm is more efficient than one at 355 nm and comparable pulse energy for standoff detection of biological aerosols that are BWA simulants. In particular, the anthrax simulants BG and BT had almost an order of magnitude stronger fluorescence, whereas the toxin simulant OA fluoresced approximately twice as strong at the shorter excitation wavelength. For the virus simulant MS2, and the *E.coli* and SM cultures of bacteria, the fluorescence responses were approximately the same in terms of magnitude for the different excitation wavelengths. Stronger fluorescence means higher sensitivity for a given excitation pulse energy. This is crucial for standoff distance and detectable concentration levels. More importantly, however, was the prominent dissimilarities between the agent spectra at the shorter excitation wavelength as compared to those at 355 nm excitation. The fluorescence spectra measured at 210 m standoff distance compare well with spectra measured in laboratory experiments or using aerosol sampling systems; except for MS2, which may be a result of poor separation from the growth medium and aerosol preparation. More distinguishable spectra allow for better classification thus lower false alarm rates, which in the end is the major challenge of standoff detection. Even better performance in terms of false alarm rate, would be an instrument utilizing two UV excitation wavelengths, as asserted by publications on laser induced fluorescence measurements on individual particle aerosols [26,27,29,30]. The standoff instrument of the present work is capable of emitting both wavelengths. Minor modifications will allow for automatic dual excitation wavelength operation.

In order to avoid problems with Raman scattering of atmospheric constituents appearing within the peak of the fluorescence spectrum, the excitation wavelength should ideally be shorter than the 294 nm used in these experiments. The advantage of moving the Raman scattering out of the fluorescence window has to be balanced by the reduced transmission in air caused by ozone pollution. An optimal excitation wavelength is probably in the 280-290 nm range. In any case, using a different excitation wavelength than one available from a commercial laser has to be traded off against the cost of generating it in terms of pulse energy and system complexity.

Acknowledgments

We acknowledge Torbjörn Tjärnhage (Swedish Defence Research Agency) for lending us the dry release equipment. We also acknowledge Arthur D. van Rheenen (FFI) for providing the MODTRAN calculations.